Kinetic Analysis of *Dictyostelium discoideum* Myosin Motor Domains with Glycine-to-Alanine Mutations in the Reactive Thiol Region†

Renu Batra,‡ Michael A. Geeves,§,|| and Dietmar J. Manstein*,‡

Max-Planck-Institut für Medizinische Forschung, Jahnstr. 29, D-69120 Heidelberg, Germany, and Max-Planck-Institut für Molekulare Physiologie, Postfach 102664, D-44026 Dortmund, Germany

Received September 18, 1998; Revised Manuscript Received February 12, 1999

ABSTRACT: Three conserved glycine residues in the reactive thiol region of *Dictyostelium discoideum* myosin II were replaced by alanine residues. The resulting mutants G680A, G684A, and G691A were expressed in the soluble myosin head fragment M761-2R [Anson, M., Geeves, M. A., Kurzawa, S. E., and Manstein, D. J. (1996) *EMBO J. 15*, 6069−6074] and characterized using transient kinetic methods. Mutant G691A showed no major alterations except for a marked increase in basal Mg^{2+}-ATPase activity. Phosphate release seemed to be facilitated by this mutation, and the addition of actin to G691A stimulated ATP turnover not more than 3-fold. In comparison to M761-2R, mutant constructs G691A and G684A showed a 4-fold reduction in the rate of the ATP cleavage step. Most other changes in the kinetic properties of G684A were small (∼2-fold). In contrast, substitution of G680 by an alanine residue led to large changes in nucleotide binding. Compared to M761-2R, rates of nucleotide binding were 20−30-fold slower and the affinity for mantADP was approximately 10-fold increased due to a 200-fold reduction in the dissociation rate constant of mantADP. The ATP-induced dissociation of actin from the acto·680A complex was normal, but the communication between ADP and actin binding was altered such that the two sites are thermodynamically uncoupled but kinetically actin still accelerates ADP release.

Cells undergo a wide variety of motile processes that are driven by molecular motors, enzymes that transduce the chemical energy of ATP hydrolysis into mechanical force and displacement. The most extensively studied motor protein is myosin II, the motor that drives muscle contraction and other essential motile processes in eukaryotic cells (*1*, *2*). The myosin head fragment, also termed subfragment-1 or S1,[1] consists of an amino-terminal head domain and a long α-helix that extends from the globular part of the head and forms a complex with the essential (ELC) and regulatory (RLC) light chains. Both actin and nucleotide binding sites are located within the globular part of the head, frequently referred to as catalytic or motor domain as it acts as an independent functional motor unit in vitro. The complex formed by the long carboxy-terminal α-helix and both light chains is referred to as the light chain binding domain (LCBD) or regulatory domain. It has been shown that replacement of the LCBD with genetically engineered domains of similar rigidity and dimensions produces functional motors with kinetic properties similar to those of the parent *Dictyostelium discoideum* myosin II (*3*). The advantages of such engineered myosin head fragments (MHFs) include high levels of expression, ease of purification, and functional competence, facilitating their use in structural and functional studies.

Here we have used one such construct, M761-2R, corresponding to amino acid residues 1−761 of the globular head domain of *D. discoideum* myosin II fused to two α-actinin repeats, to study mutations in the reactive thiol region. This well-conserved region corresponds to a bent α-helix situated in the lower part of the motor domain, between the nucleotide binding site and the regulatory domain. In skeletal muscles this region contains two reactive sulfhydryls SH1 and SH2, corresponding to C707 and C697 in the chicken myosin heavy chain sequence.

It was suggested that changes in the nucleotide state of the active site lead to conformational changes in the reactive thiol region (*4*). The two sulfhydryls in this region can be cross-linked by a variety of reagents bridging distances of 2−18 Å (*5*−*7*). Myosin with SH1 and SH2 cross-linked within a distance of 3 Å is predicted to hold the nucleotide "trapped" in the active site with no measurable ATPase activity (*8*). Chemical modification of SH1 and SH2 resulted in dramatic alteration of myosin ATPase activity and actin binding affinity, and nucleotide binding alters the separation between SH1 and SH2 (*9*, *10*). The reactive thiol helix of *D. discoideum* myosin II contains three glycine residues

† Supported by the Max-Planck-Society.

* To whom correspondence should be addressed. Tel: (+49-6221) 486 212. Fax: (+49-6221) 486 437. E-mail: manstein@mpimf-heidelberg.mpg.de.

‡ Max-Planck-Institut für Medizinische Forschung.

§ Max-Planck-Institut für Molekulare Physiologie.

|| Current address: Department of Biosciences, University of Kent, Canterbury, Kent, U.K.

[1] Abbreviations: ATP, adenosine-5′-triphosphate; DTT, 1.4-dithiothreitol; EDTA, ethylenediamine tetraacetic acid; EGTA, ethyleneglycol-bis-(2-aminoethyl ether)-*N*,*N*,*N*′,*N*′-tetraacetic acid; kb, kilobase(s); HMM, heavy meromyosin; M761-2R, recombinant protein corresponding to myosin catalytic domain fused to two α-actinin repeats; MHF, myosin head fragment; MHC, myosin heavy chain; mantADP, 2′ (3′)-*O*-(*N*-methylanthraniloyl)-ADP; *mhc*A, gene encoding MHC; MOPS, 3-(*N*-morpholino)-propanesulfonic acid; PCR, polymerase chain reaction; pyr-actin, actin labeled with pyrene iodoacetamide on Cys-374; S1, subfragment 1 of myosin.

10.1021/bi982251e CCC: $18.00 © 1999 American Chemical Society
Published on Web 04/20/1999

corresponding to G680, G684, and G691 (corresponding to residues 699, 703, and 710 in chicken skeletal myosin), and one of the thiol positions (SH1) is occupied by a threonine residue (T688). A bend in the helix occurs at residue C678 (SH2), close to an absolutely conserved glycine (G680), and the helix ends with a second absolutely conserved glycine (G691). A third glycine (G684) is conserved among the class II myosins. It was suggested that these glycines act as swivels or fulcrums and that their replacement by bulkier residues may block transition between conformations occurring during the motor cycle and trap the motor in otherwise short-lived states (*6*). Winkelmann and co-workers reported the mutation of G699 of chicken skeletal myosin (corresponding to G680 in *D. discoideum*) to alanine, resulting in a more than 100-fold reduction in the ability of the mutant protein to support filament sliding in vitro (*11*). Similar results were obtained with mutants G680V and G691V of *D. discoideum* myosin II (*12*). In both studies, it was shown that replacement of G680 (or the equivalent residue in chicken skeletal myosin) with a bulkier residue results in low ATPase activities and has a dominant effect on actin filament sliding in vitro. Filament movement in assays with 9:1 mixtures of wild-type and mutant motor domains resembled that of a pure mutant population (*11*, *12*).

In the present work we used an integrated molecular genetic and kinetic approach to investigate the role of the three conserved glycine residues in the reactive thiol region of *D. discoideum* myosin II. Glycine to alanine changes were obtained at each position by site-directed mutagenesis. Our results showed that replacing G680 with alanine produces a long-lived actomyosin·ADP complex. A detailed transient kinetic characterization of the changes showed that the G680A construct has a 30-fold slower ATP binding rate, an 11-fold higher affinity for ADP, an 8−10-fold slower basal ATPase rate, and a 5-fold higher affinity for actin. The acto·G680A complex has a 180-fold higher affinity for ADP. In contrast, alanine mutagenesis of G684 and G691 resulted in few changes in their transient kinetic properties. No constant changed by more than a factor of 3 except for a 4−5-fold reduction in the ATP cleavage rate constant for both constructs and a 10-fold higher affinity of ATP for acto·G684A. G691A showed a marked elevation of basal ATPase activity and little activation upon the addition of actin.

MATERIALS AND METHODS

Plasmid Construction and Mutagenesis. Molecular cloning techniques were performed as described in Sambrook et al. (*13*). Enzymes were obtained from Boehringer Mannheim and New England Biolabs. *Escherichia coli* strain XL1Blue (Stratagene, Heidelberg) was used for the amplification of plasmids. The expression vectors used for the production of mutant myosin constructs were based on pDXA-3H (*14*) and were created as described earlier (*3*). The point mutations were introduced in M761-2R, a fusion construct comprising the first 761 residues of the *D. discoideum-mhcA* gene linked to codon 264 extending to 505 of the *D. discoideum* α-actinin gene. All constructs were tagged at their C-terminus with the peptide Asp-Ala-Leu-$(His)_8$. Plasmids encoding M761-2R with glycine to alanine mutations were created by site-directed mutagenesis using the Quick-change kit obtained from Stratagene, Germany. The oligonucleotides used to PCR the myosin mutants were the following: **G680A** (5′CTCGACCAATTACGTTGCAATG*C*TGTCCTCGAAGGTATCGTATTAC), **G684A** (5′GTTGCAATGGTGTCCTCGAAG*C*TATTCGTATTACTCGTAAAGGTTTC), and **G691A** (5′CGAAGGTATTCGTATTACTCGTAAAG*C*TTTCCCAAATCGTATTATCTATGC) with the mutated residues in italics. All myosin constructs were confirmed by sequencing.

Strains and Growth Conditions. D. discoideum transformants were grown at 21 °C in HL-5C containing (per liter): 5 g of protease peptone (Merck), 5 g of Bacto yeast extract (Difco), 2.5 g of Bacto tryptone (Difco), 2.5 g of casein peptone (Merck), 10 g of D-glucose, 0.35 g of Na_2HPO_4, and 1.2 g of KH_2PO_4 (pH 6.5). Cells were grown either on 9 cm plastic Petri dishes or in 100 mL conical flasks on a gyratory shaker at 190 rpm. Plasmids were transformed into Orf^+ cells by electroporation (*14*, *15*). Transformants were selected and continuously grown in the presence of 10 μg/mL of the aminoglycoside G418 (Gibco BRL). Transformants were screened for the production of the recombinant myosin motor domains as described previously (*16*).

Protein Purification. Cells producing the wild-type and mutant myosin motor domains were grown in 5 L flasks containing 2.5 L of HL-5C. The flasks were incubated on gyratory shakers at 190 rpm and 21 °C. Cells were harvested at a density of about 5.5×10^6 mL^{-1} by centrifugation for 7 min at 2400 rpm in a Beckman J-6 centrifuge and washed once in phosphate-buffered saline. The His-tagged motor domains were purified as described by Manstein and Hunt (*16*). The purified protein could be stored at −80 °C for several months without apparent loss of enzymatic activity.

Rabbit skeletal muscle actin was purified by the method of Lehrer and Kewar (*17*). The preparation of pyrene-labeled actin was as previously described (*18*). Bradford's assay was used for the determination of protein concentration taking BSA as standard (*19*).

Stopped-Flow Experiments and Fluorescence Titration. Stopped-flow experiments were performed for transient kinetic measurements at 20 °C with a Hi-Tech SF61 stopped-flow spectrophotometer equipped with 100 W Xe/Hg lamp and a monochromator. Pyrene- and mant-fluorescence were excited at 365 and 366 nm, respectively, and detected after passing through a KV 389 nm cutoff filter. Tryptophan fluorescence, excited at 290 nm, was monitored through a WG 320 nm cutoff filter. Data were stored and analyzed using software provided by Hi-Tech Scientific (Salisbury, U.K.). Transients shown are the average of three to five consecutive shots made on the stopped-flow machine. All concentrations refer to the concentration of the reactants after mixing in the stopped-flow observation cell. Typically working volumes of 700 μL were used to obtain one data set. The data obtained with the mutants are compared with the original data obtained with M761-2R referred to as wild type in this work. Unless mentioned otherwise, the experimental buffer was 20 mM MOPS, 5 mM $MgCl_2$, and 100 mM KCl (pH 7.0).

Transient Kinetic Properties of the MHF Constructs. Previous studies of M761-2R have shown that the interaction of this construct with nucleotide and actin follows the same basic mechanism that was described for S1 from rabbit fast skeletal muscle myosin and other muscle myosins (*20*). Therefore, the dynamics of ATP binding and hydrolysis by

Scheme 1

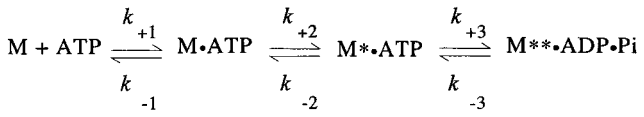

Scheme 2

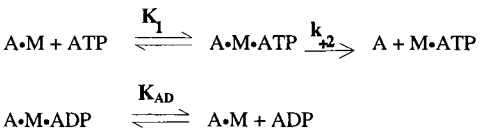

Scheme 3

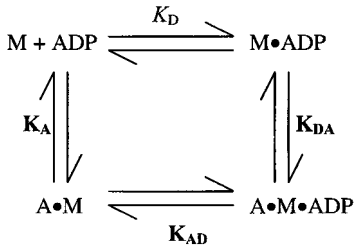

the myosin constructs were analyzed in terms of the model shown in Scheme 1 based on that of Bagshaw et al. (*21*). In this and the following schemes a notation is used that distinguishes between the constants in the presence and absence of actin by using bold ($\mathbf{k_{+1}}$, $\mathbf{K_1}$) versus italic type (k_{+1}, K_1); subscripts A and D refer to actin ($\mathbf{K_A}$) and ADP (K_D), respectively.

Asterisks represent different protein conformations as detected by intrinsic protein fluorescence, and K_i for the *i*th step is defined as the association constant ($=k_{+i}/k_{-i}$). Experiments in the presence of actin were analyzed in terms of models developed by Millar and Geeves (*22*) and Siemankowski and White (*23*). In this scheme (Scheme 2) A and M represent actin and myosin motor domain construct, respectively.

A rapid equilibrium is reached between A·M and ATP after mixing acto·MHF and ATP, defined by the association constant $\mathbf{K_1}$, followed by isomerization of the ternary complex which limits the maximum rate of actin dissociation from the complex. Thus the observed rate constant for the ATP-induced dissociation of actin is defined by

$$k_{obs} = [ATP]\mathbf{K_1}\mathbf{k_{+2}}/(1 + \mathbf{K_1}[ATP]) \quad (1)$$

In the presence of ADP, the two nucleotides compete to bind to A·M. Assuming a rapid equilibrium between A·M and the ADP bound state, k_{obs} for a fixed ATP concentration is given by the equation

$$k_{obs} = k_0/(1 + [ADP]/\mathbf{K_{AD}}) \quad (2)$$

where k_0 is the observed rate constant in the absence of ADP and dissociation constant $\mathbf{K_{AD}}$ represents the affinity of ADP for the actomyosin complex (*23*).

Scheme 3 illustrates coupling between actin and the nucleotide binding site. In this scheme all constants are defined as dissociation constants. The presence of actin alters the affinity of ADP for myosin and vice versa. The ADP affinity for MHF is given as K_D, and the affinity of myosin for actin is defined as $\mathbf{K_A}$. In forming the ternary A·M·ADP complex both the affinity of actin for myosin ($\mathbf{K_{DA}}$) and the affinity of ADP for myosin ($\mathbf{K_{AD}}$) are weakened (*24*).

Table 1: Steady-State ATPase Activities of Mutant and Wild-Type Myosin Head Fragments[a]

MHF construct	basal Mg^{2+} ATPase (s^{-1})	high-salt Ca^{2+} ATPase (s^{-1})	actin-activated Mg^{2+}-ATPase		
			K_{app} (μM)	k_{cat} (s^{-1})	k_{cat}/K_{app} ($M^{-1}\,s^{-1}$)
M761-2R	0.12	1.1	110	2.7	0.25×10^5
G680A	0.02	0.1	140	2.1	0.15×10^5
G684A	0.20	1.0	120	3.6	0.3×10^5
G691A	0.48	0.9	40	1.2	0.3×10^5

[a] All measurements were performed at 30 °C. Experimental conditions for all measurements are as described in the Methods section.

Determination of ATPase Activity. Steady-state ATPase assays were performed as described previously (*17*, *25*). The values for k_{cat}/K_{app} were calculated from the initial slope of the data fit to the Michaelis−Menten equation. Estimates of the individual Michaelis−Menten parameters were obtained from double-reciprocal plots. Additionally, ATPase assays were performed in the presence of 0.5−10 mM ATP to confirm that the amount of ATP was not rate-limiting for the mutant myosin constructs.

RESULTS

Protein Purification. High synthesis levels were obtained with M761-2R and all of the mutant constructs described in this study. The histidine-tagged recombinant proteins were purified to homogeneity by binding to actin and release with ATP followed by Ni^{2+} chelate affinity chromatography. An average yield of 2 mg of myosin head fragment was obtained per gram of cells. The purified proteins were >95% pure as estimated from the Coomassie blue-stained SDS−polyacrylamide gel. The mutant constructs did not behave significantly different from wild-type construct M761-2R in this purification.

Steady-State ATPase Assays. Hydrolysis of ATP by the wild-type and the mutant myosin constructs was measured under three different conditions, namely, basal ATPase, actin-activated ATPase, and high-salt Ca^{2+} ATPase. The first two were measured under low salt and in the presence of Mg^{2+} (Table 1). Basal ATPase activity of M761-2R was 0.12 s^{-1}, and that of mutant G684A was 0.2 s^{-1}. Mutant G680A has a reduced basal ATPase activity of 0.02 s^{-1}, while mutant G691A showed an elevated basal ATPase activity of 0.48 s^{-1}. High-salt Ca^{2+} ATPase rates measured for G684A, G691A, and M761-2R were similar, while G680A gave a 10-times slower high-salt Ca^{2+} ATPase rate.

Activation of ATPase activity by actin was examined over a wide range of actin concentrations (0−50 μM). At concentrations of actin much lower than K_{app}, the dependence of the apparent ATPase rate on actin concentration could be fit to a straight line and the apparent second-order rate constant (k_{cat}/K_{app}) of the reaction could be determined from the slope of this line. Estimates of K_{app} and k_{cat} were obtained from double-reciprocal plots (Table 1), but as the maximum actin concentrations accessible were below the estimated value of K_{app}, the values must be treated with some caution.

Table 2: Transient Kinetic Analysis of Nucleotide Binding to Myosin Head Fragments[a]

nucleotide	rate constant	M761-2R	G680A	G684A	G691A
ATP	K_1k_{+2} (M^{-1} s^{-1})	1.1×10^6	3.5×10^4	0.5×10^6	1.1×10^6
	$k_{+3} + k_{-3}$ (s^{-1})	45	44	8.2	11
mantADP	k_{+D} (M^{-1} s^{-1})	6.7×10^5	0.4×10^5	5×10^5	6×10^5
	k_{-D} (s^{-1})	2.60	0.01	0.88	1.62
	K_D (μM)[b]	3.90	0.25	1.76	2.70
ADP	K_D (μM)[c]	14	1.3	7	9

[a] Experimental conditions for all measurements: 20 mM MOPS, 5 mM $MgCl_2$, and 100 mM KCl (pH 7.0), 20 °C. [b] Calculated value (k_{-D}/k_{+D}). [c] Dissociation rate constant for ADP measured from ADP inhibition of pyr-actin binding to MHF.

ATP and mantATP Binding to MHF (K_1k_2, $k_{+3} + k_{-3}$). Binding of mantATP to mutant myosin head fragments was monitored from the 2.2-fold increase in fluorescence observed following the addition of substoichiometric concentrations of mantATP to each construct. The observed process could be fit to a single exponential [$F = F_o(1 - e^{-k_{obs}t})$]. The observed rate constant (k_{obs}) values were linearly dependent on the concentration of mantATP in the range 5−25 μM. The second-order rate constant (K_1k_{+2}) is defined by the slope of the best-fit line (data not shown); values of K_1k_{+2} were similar for M761-2R and G691A but 30- and 2-fold slower for G680A and G684A (Table 2).

Binding of ATP was monitored by the change in intrinsic protein fluorescence following the addition of excess of ATP. A 9% increase in fluorescence was observed for all myosin constructs, and the observed process was analyzed as described for mantATP binding. Values of k_{obs} obtained with ATP in the range 5−100 μM were similar to those obtained for mantATP binding in the 5−25 μM range. At higher concentrations of ATP (>1 mM), k_{obs} values were no longer linearly dependent upon [ATP] and were best fit to a hyperbola ($k_{obs} = k_{max}[ATP]/([ATP] + K_{0.5})$) (Figure 1A). For S1, the plateau of the hyperbola was assigned to the rate for the ATP cleavage step ($k_{+3} + k_{-3}$) and the second-order rate constant to K_1k_{+2}. We assume that the same assignment holds for the *D. discoideum* myosin motor domain. G684A and G691A gave similar values for the rate of the cleavage step, and both mutants are about 4-fold slower than M761-2R. In contrast, the value obtained for G680A was similar to that obtained for M761-2R. Previously, we have reported similar variability in $k_{+3} + k_{-3}$ values with various myosin head fragments showing otherwise similar kinetic behavior (*20*). According to Scheme 1, a strict hyperbolic dependence of k_{obs} upon ATP concentration is not expected, since ATP binding is presumed to be a rapid, almost irreversible phenomenon. Therefore, $K_{0.5}$ defines the ATP concentration at which $K_1k_{+2}[ATP] \approx (k_{+3} + k_{-3})/2$. At ATP concentrations in the range from 5 to 100 μM, the apparent second-order rate constant for ATP binding to myosin head fragments (K_1k_{+2}) was in agreement with the calculated values obtained from $k_{max}/K_{0.5}$. Once again, the values were similar for M761-2R, G684A, and G691A but 30-fold lower for mutant G680A.

Binding of mantADP to Myosin Head Fragments (k_{+D}). Binding of mantADP to myosin head fragments was monitored by observing the exponential increase in fluorescence. The observed rate constants were linearly dependent on the concentration of mantADP over the range 5−50 μM. The second-order rate constant was measured from the slope of the plot obtained in Figure 1B. The values obtained for M761-2R, G684A, and G691A were similar, while the

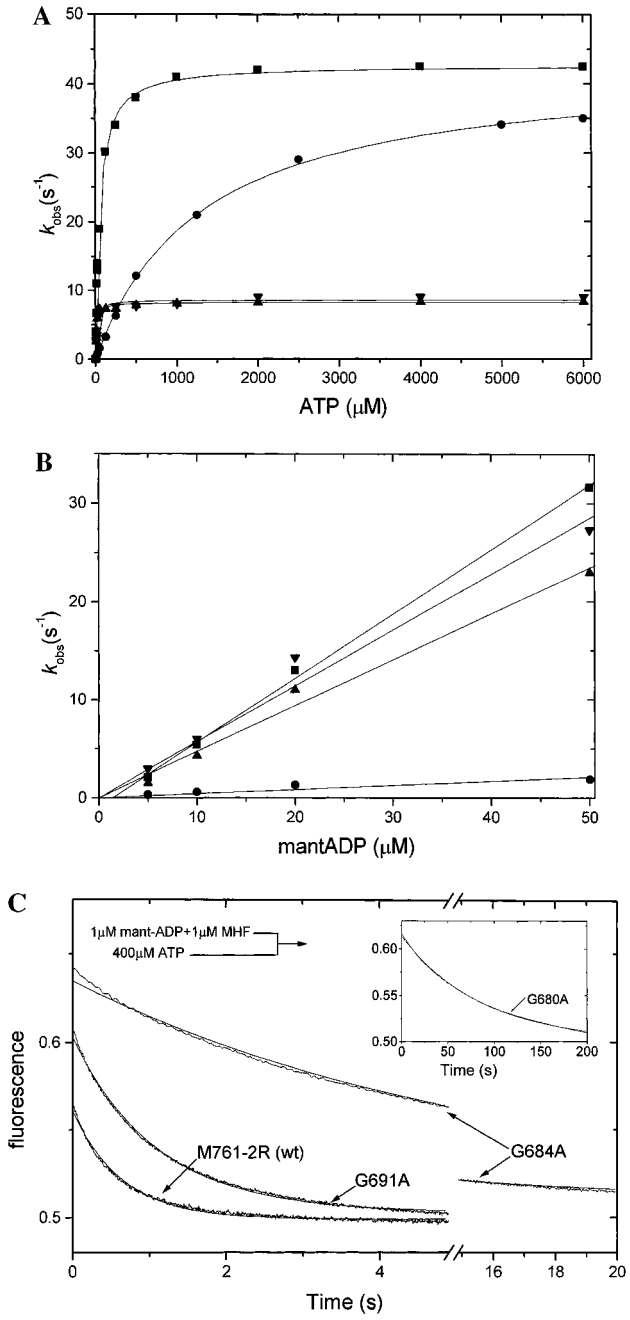

FIGURE 1: Binding of ATP and mant-nucleotides to myosin head fragments. (A) Rate of ATP binding to myosin head fragments. Dependence of the observed rate constant of fluorescence change on [ATP] in the range 0.1−6 mM. Data were fit to a hyperbola as described in text. The resulting rate constants are summarized in Table 2. The second-order rate constants (K_1k_2) were similar for ATP and mantATP binding. (B) Binding of mantADP to myosin head fragments. Dependence of the observed process on mantADP concentration (5−50 μM). The data were fit to a straight line, with the second-order rate constant of ADP binding (k_{+D}) defined by the slope of the line. (D) Rate of ADP displacement from myosin head fragments. Stopped-flow record of fluorescence decrease upon binding of 400 μM ATP to 1.0 μM MHF, premixed with 1 μM mantADP. The observed rate constants (k_{-D}) are summarized in Table 2. The symbols correspond to the *D. discoideum* myosin head fragments M761-2R (■), G680A (●), G684A (▲), and G691A (▼). Buffer conditions: 20 mM MOPS, 5 mM $MgCl_2$, and 100 mM KCl (pH 7.0), 20 °C.

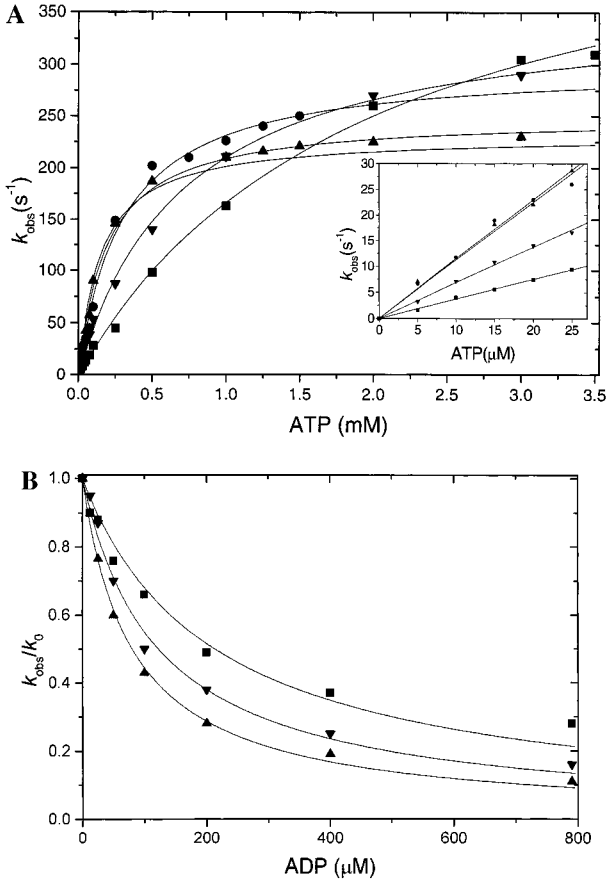

FIGURE 2: ATP-induced dissociation of the pyr-acto·MHF complexes. (A) Determination of the maximum rate of ATP binding to pyr-acto·MHF. Data over the range from 0.005 to 3.5 mM ATP were fitted to a hyperbolic function. The rate constants for the isomerization step are given by the plateau values. The observed rate constant is linearly dependent on ATP concentrations in the range 5−25 μM (insert). The fitted parameters are summarized in Table 3. (B) Plot of k_{obs}/k_0 versus [ADP]: competitive binding of ATP and ADP to pyr-acto·MHF. The dissociation constants of the ADP complexes were determined by fitting the plot to the equation $k_{obs}/k_0 = 1/(1 + [ADP]/\mathbf{K_{AD}})$, where k_0 corresponds to the observed rate constant in the absence of ADP. The symbols correspond to the *D. discoideum* myosin fragments M761-2R (■), G680A (●), G684A (▲), and G691A (▼). Buffer conditions: 20 mM MOPS, 5 mM $MgCl_2$, and 100 mM KCl (pH 7.0), 20 °C.

rate constant measured for G680A was 16-fold slower (Table 2).

ADP Dissociation from Myosin Head Fragments (k_{-D}). The rate of mantADP dissociation was measured by monitoring the decrease in fluorescence upon displacement of mantADP from the MHF·mantADP complex by the addition of excess ATP. The rate of mantADP release (k_{-D}) from G680A, G684A, and G691A was 260-, 3-, and 1.6-fold slower than the rate measured for M761-2R (Figure 1C, Table 2).

ATP-Induced Dissociation of acto·MHF ($\mathbf{K_1k_{+2}}$). Binding of ATP to pyr-acto·MHF complexes was monitored by observing the exponential increase in pyrene fluorescence as the complex dissociates upon addition of excess ATP. The observed rate constants were linearly dependent upon ATP concentration in the range from 5 to 25 μM, and the second-order rate constants, $\mathbf{K_1k_{+2}}$, are defined by the slopes of the best-fit lines shown in Figure 2A (insert). The values of $\mathbf{K_1k_{+2}}$ obtained for the mutant constructs differed by a factor of 2−3 from the wild-type value. At higher concentrations of ATP, the rate constants were no longer linearly dependent on ATP concentration and could be fit to a hyperbola as predicted from Scheme 2 and eq 1 (Figure 2A). The values obtained for $\mathbf{k_{+2}}$ for the mutant myosin constructs and M761-2R were comparable. This indicates that the mutations primarily affect $\mathbf{K_1}$, and consequently, ATP binds more tightly to the acto·MHF complexes of the mutant constructs G680A and G684A than to the respective myosin head fragments alone.

ADP Inhibition of ATP-Induced Dissociation of acto·MHF (K_{AD}). The affinity of ADP for pyr-acto·MHF was determined from the inhibition of ATP-induced dissociation of pyr-acto·MHF as described by eq 2. The observed rate of dissociation was reduced for all constructs when excess ATP was added to pyr-acto·MHF with varying concentrations of ADP (Figure 2B). The reaction was monophasic for M761-2R, G684A, and G691A. The data obtained for these constructs were fit to eq 2 and gave values of 215, 82, and 125 μM for M761-2R, G684A, and G691A, respectively.

In contrast, the presence of small amounts of ADP in pyr-acto·G680A produced biphasic dissociation reactions (Figure 3A). Over the concentration range 0−4 μM ADP, k_{obs} values for the two phases were independent of the ADP concentration with the fast phase being identical to the k_{obs} in the absence of ADP. The slow phase was 3.1 s^{-1}. The amplitude of the 2 phases varied with ADP concentration as shown in Figure 3B, being entirely fast phase at zero [ADP] and entirely slow phase at [ADP] > 10 μM. The [ADP] dependence of the amplitudes could be described by hyperbolic functions as shown in Figure 3B. The fraction of pyr-acto·G680A that is free of ADP dissociated at 40 s^{-1} (k_{obs} in the absence of ADP), which in turn was the rate of ATP binding. The fraction of pyr-acto·G680A that has ADP bound dissociated at a rate limited by the rate of ADP dissociation (3.1 s^{-1}). The data are thus compatible with a titration of pyr-acto·G680A by ADP with a $\mathbf{K_{AD}}$ of 1.2 μM. Thus ADP binds tightly to acto·G680A with a slow rate of ADP release. The values of $\mathbf{K_{AD}}$ and $\mathbf{k_{+AD}}$ give an association rate constant for ADP of $\mathbf{k_{+AD}} = \mathbf{k_{-AD}}/\mathbf{K_{AD}} = 2.6 \times 10^6$ M^{-1} s^{-1}.

The tight binding of ADP to acto·G680A suggests that ADP competes efficiently with ATP for the actomyosin-binding site. To test this further, we examined the ATP-induced dissociation of acto·G680A by premixing 50 μM ATP with various concentrations of ADP. As in the experiment where ADP was premixed to acto·G680A, the presence of ADP produced two phases. The amplitude of the fast phase decreased and the slow phase increased with an increase in ADP concentration, and the two amplitudes were equal in size at approximately 20 μM ADP. The reduction in k_{obs} of the slow phase with increasing ADP concentration is a measure of efficiency with which ATP replaced the ADP that dissociated from acto·G680A. The k_{obs} of the slow phase (Figure 3C) and analysis of the amplitudes suggest that 20 μM ADP and 50 μM ATP bound to acto·G680A with equal rates; the second-order rate constant for ADP binding was approximately 2.5 times higher than that of ATP. This conclusion is also supported by the analysis of the observed rate constant of the fast phase that increased linearly with increasing [ADP] (Figure 3D). For a model where ADP binding and ATP binding are essentially irreversible on the time scale of the fast phase, k_{obs}(fast phase) = k_T[ATP] +

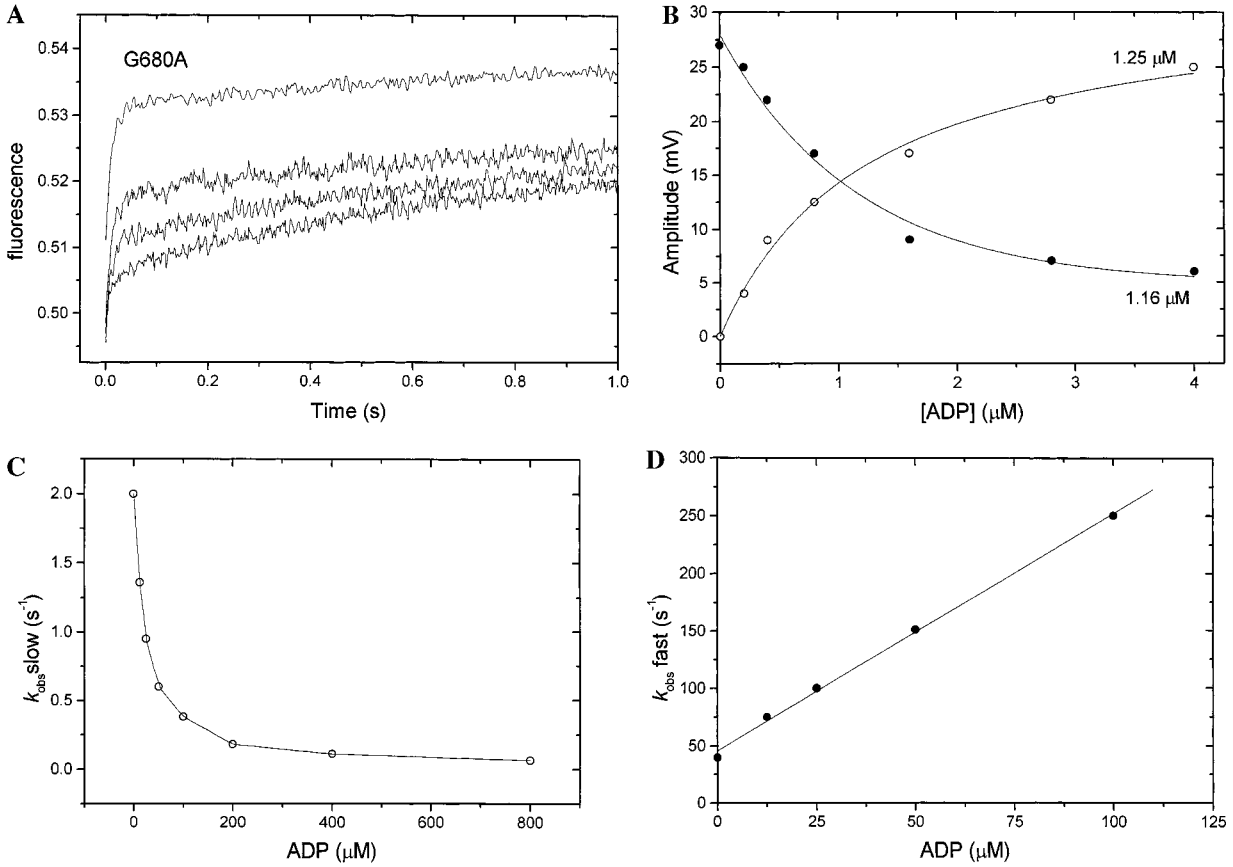

FIGURE 3: ADP inhibition of ATP-induced dissociation of the pyr-acto·G680A complex. (A) Fluorescence changes observed when 100 μM ATP is mixed with 0.5 μM acto·G680A premixed with ADP concentrations of 0.1, 0.2, 0.4, and 0.8 μM. The dissociation reaction shown is biphasic. (B) [ADP] dependence of the observed amplitudes of the dissociation reaction with mutant myosin G680A. The best fits to the hyperbola are superimposed and give $\mathbf{K_{AD}}$ values of 1.25 and 1.16 μM for the slow (○) and fast (●) phases, respectively. The observed rate constants for the slow and fast phases for mutant G680A are plotted in panels C and D. The results are summarized in Table 3. Buffer conditions: 20 mM MOPS, 5 mM $MgCl_2$, and 100 mM KCl (pH 7.0), 20 °C.

Table 3: Results of the Transient Kinetic Analysis of the Actomyosin Complexes[a]

nucleotide	rate constant	M761-2R	G680A	G684A	G691A
		Nucleotide Binding to acto·MHF			
ATP	$\mathbf{K_1k_{+2}}$ (M^{-1} s^{-1})	1.55×10^5	5.5×10^5	5.5×10^5	3.1×10^5
	$\mathbf{K_1}$ (M^{-1})	250	1515	2500	685
	$\mathbf{k_{+2}}$ (s^{-1})	504	310	255	365
ADP	$\mathbf{K_{AD}}$ (μM)	215	1.2	82	125
	$\mathbf{k_{+AD}}$ (M^{-1} s^{-1})[b]	nd	2.6×10^6	nd	nd
	$\mathbf{k_{-AD}}$ (s^{-1})	>100	3.1	>50	>90
	$\mathbf{K_{AD}}/K_D$	14.3	0.92	11.5	13.9
		Actin Binding to MHF			
	$\mathbf{k_{+A}}$ (M^{-1} s^{-1})	1.3×10^6	0.5×10^6	1.1×10^6	1.0×10^6
	$\mathbf{k_{-A}}$ (s^{-1})	5.6×10^{-3}	0.4×10^{-3}	14.0×10^{-3}	1.4×10^{-3}
	$\mathbf{K_A}$ (nM)[b]	4.3	0.8	13.2	1.4
	$\mathbf{K_{DA}} = \mathbf{K_A K_{AD}}/K_D$ (nM)[b]	61.5	0.7	151.8	19.5
	$\mathbf{k_{+DA}}$ (M^{-1} s^{-1})	0.19×10^6	0.14×10^6	0.21×10^6	0.18×10^6
	$\mathbf{k_{-DA}}$ (s^{-1})[b]	11.7×10^{-3}	0.1×10^{-3}	32×10^{-3}	$3.5 \times 1\,0^{-3}$
	$\mathbf{k_{-DA}}/\mathbf{k_{-A}}$	2.0	0.25	2.2	2.5

[a] Experimental conditions for all measurements: 20 mM MOPS, 5 mM $MgCl_2$, and 100 mM KCl (pH 7.0), 20 °C. [b] Calculated values; nd, not determined.

k_D[ADP], where k_T and k_D are the apparent second-order rate constants of ATP and ADP binding, respectively. The slope of the fitted line gives a second-order rate constant of ADP binding of 2.6×10^6 M^{-1} s^{-1} compared to 1×10^6 M^{-1} s^{-1} for ATP (Figure 3D, Table 3).

Actin Binding to Mutant Myosin Head Fragments ($\mathbf{k_{+A}}$). The rate of actin binding was measured by following the exponential decrease in pyrene fluorescence observed upon binding of excess pyr-actin to myosin head fragments (*27*). The observed rate constants were plotted against the pyr-actin concentration, and in each case k_{obs} was linearly dependent upon actin concentration over the range studied (0.5−3.0 μM) (Figure 4A). This is compatible with a simple one-step binding mechanism (Scheme 3), where $k_{obs} = [A]\mathbf{k_{+A}} + \mathbf{k_{-A}}$. The values of the second-order rate constants of pyr-actin binding ($\mathbf{k_{+A}}$) obtained from the slopes

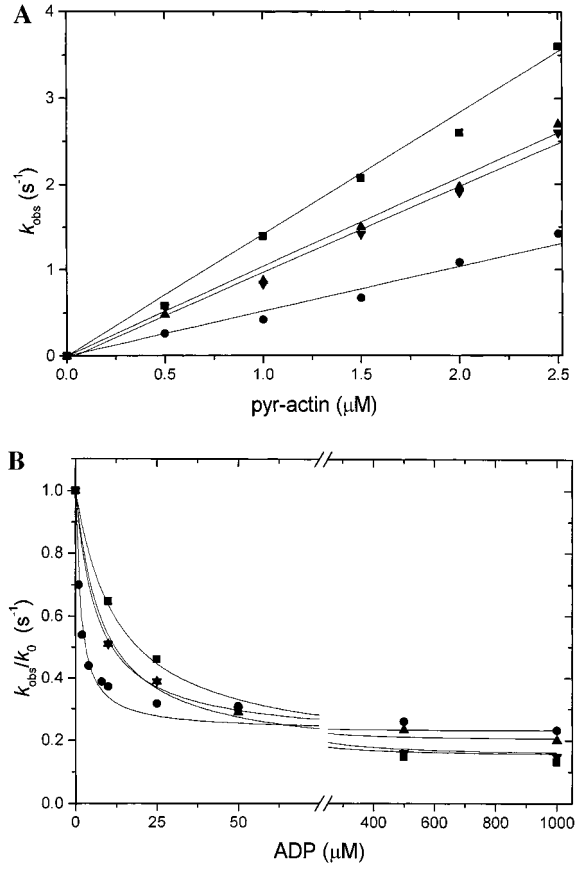

FIGURE 4: Interaction of pyr-actin with myosin head fragments. (A) Dependence of the rate of pyr-actin binding to myosin head fragments on pyr-actin concentration. The data were fit to a straight line, the slope of which gives the second-order rate constants for binding to actin ($\mathbf{k}_{+A}$). All of the resulting values are summarized in Table 3. (B) ADP inhibition of the rate of pyr-actin (8 μM) binding to myosin head fragments. The dissociation constants of the MHF·ADP complexes were determined by fitting the plot $k_{obs}/\mathbf{k}_{+A}$ vs ADP concentrations according to eq 3. The symbols correspond to the *D. discoideum* myosin head fragments M761-2R (■), G680A (●), G684A (▲), and G691A (▼). Buffer conditions: 20 mM MOPS, 5 mM $MgCl_2$, and 100 mM KCl (pH 7.0), 20 °C.

of the plots were almost identical for the mutant constructs and M761-2R (Table 3). The intercept, $\mathbf{k}_{-A}$, was too small to estimate in each case.

Displacement of pyr-actin from pyr-acto·MHF ($\mathbf{k}_{-A}$). The rate of actin dissociation ($\mathbf{k}_{-A}$) from the myosin constructs was determined by displacing pyr-actin from pyr-acto·MHF with an excess of unlabeled actin. The observed process could be fit to a single exponential where k_{obs} corresponds directly to $\mathbf{k}_{-A}$. The rate of actin dissociation measured for mutant constructs G680A and G691A was 10- and 4-fold slower than for M761-2R, while G684A showed a slight increase in the rate of actin dissociation (Table 3). The dissociation equilibrium constants for actin binding ($\mathbf{K}_A$) show that the actin affinities of constructs G680A and G691A are 5- and 3-fold lower than the value obtained for M761-2R.

ADP Inhibition of Pyr-Actin Binding to MHF (K_D, $\mathbf{k}_{+DA}$). In the presence of ADP, the rate of actin binding was reduced more than 10-fold for many myosins and this is also true for the constructs used here (data not shown). Studies of 8 μM pyr-actin binding to 0.5 μM myosin construct showed an exponential decrease in pyr-actin fluorescence, and as stated above, $k_{obs} = [A]\mathbf{k}_{+A} + \mathbf{k}_{-A}$ was 5.7, 4.5, 4.5, and 2.5 s^{-1} for M761-2R, G691A, G684A, and G680A, respectively. A single-exponential reaction was also observed in the presence of saturating concentrations of ADP, and k_{obs} values were reduced to 0.76, 0.72, 0.85, and 0.55 M^{-1} s^{-1} for M761-2R, G691A, G684A, and G680A respectively, where $k_{obs} = [A]\mathbf{k}_{+DA} + \mathbf{k}_{-DA}$ (see Scheme 3). The reduction in k_{obs} as a function of ADP concentration provides a convenient way to measure the affinity of ADP for the myosin head.

Assuming that $\mathbf{k}_{-DA} \ll [A]\mathbf{k}_{+DA}$ and that ADP is in rapid equilibrium with the myosin head fragments on the time scale of the measurements, one would expect a single exponential at all ADP concentrations where

$$k_{obs} = [A]\mathbf{k}_{+A}(K_D/\{K_D + [ADP]\}) + [A]\mathbf{k}_{+DA}([ADP]/\{K_D + [ADP]\}) \quad (3)$$

and K_D is the affinity of ADP for myosin (Scheme 3). A single exponential was observed in all cases, and the k_{obs} values plotted against the ADP concentration are shown in Figure 4B. The fit to eq 3 is superimposed in Figure 4B, giving K_D values for the mutants G680A, G684A, and G691A that are 11-, 2-, and 1.5-fold lower than the value of 14 μM obtained for M761-2R (Table 2).

DISCUSSION

In this study we used steady-state and transient kinetics to analyze the effect of mutations G680A, G684A, and G691A on nucleotide binding, actin binding, and communication between nucleotide and actin binding sites of the myosin head fragment. Mutant motor domain G691A showed no major changes except for a 4-fold reduction in the rate at which ATP cleavage occurs, as well as an increase of the basal ATPase. The change in basal ATPase suggests an increase in the phosphate release rate or the rate of the conformational change opening myosin's "back door", which limits phosphate release. Furthermore, the presence of actin failed to accelerate phosphate release by more than 3-fold. The interaction of G691A with actin or nucleotide appeared unperturbed in all other aspects studied. Thus in some way the glycine to alanine substitution at this position interferes with the ATP cleavage step and facilitates phosphate release in the absence of actin. These observations are compatible with the results reported by Patterson et al. (*12*), in which a full-length myosin construct with a glycine to cysteine substitution at position 691 showed elevated basal ATPase and actin had little effect on ATP turnover. The ability of G691C myosin to support actin filament sliding was reduced but not in a dominant way; that is, the mutant has no braking effect on motility supported by wild-type myosin (*12*).

Comparison of the crystal structures of the myosin motor domain complexed with ADP·BeF_3 (lever down) and ADP·V_i (lever up) shows significant rearrangements around G691, with some of the largest rotations within the reactive thiol region occurring in the Ψ-bond of G691 and the Φ-bond of neighboring residue K690 (*28*, *29*). In the ADP·V_i structure, G691 is in an unusual conformation that may not be accessible to alanine. In the ADP·BeF_3 structure G691 is clearly part of the helix, a conformation that is presumably also available to alanine. The observation that mutation

G691A has no effect on nucleotide binding, actin binding, or the relationship between the two, yet does disturb phosphate release and motility suggests that it lies on a communication pathway between the phosphate "back door" and the movement of the converter and the lever arm. G691 is clearly not involved in nucleotide- or actin-induced conformational changes within the motor domain; however, we cannot exclude an additional effect of mutations at this site on the mechanical coupling between motor domain and lever arm.

Mutant construct G684A showed small changes in most of its properties, for example, a 3-fold reduction in actin affinity and a 4-fold reduction in the rate of ATP cleavage. This result is in good agreement with the structural data that are available as the residue is part of an α-helix in both the ADP·V_i and ADP·BeF_3 structures and seems to undergo only minor rearrangements between the "lever up" and "lever down" states. Structural data also indicate that substitution of G684 by a larger, bulkier residue can be accommodated.

Among the three mutant constructs examined, G680A showed the most severe deviation from wild-type behavior in its transient kinetic properties. Mutations at this position were recovered by Patterson and co-workers in a screen of cold-sensitive myosin mutants (*30*, *31*), and a myosin with a glycine to alanine mutation at an equivalent position was produced as a three-part chimera in a mouse myogenic cell line myosin (*11*). Steady-state kinetics and in vitro motility assays showed a slight inhibition of the mutant proteins basal and actin-activated ATPase, a 10−100-fold reduction of its ability to support actin filament sliding, and a strong braking effect on motility supported by wild-type myosin (*11*, *12*). Mixtures containing 10% G680A or G680V strongly resembled the pure mutant population. Mutant G680V was found to have the same affinity for ADP and ATPγS, and the affinity of the mutant for nucleotide was found to be 40-fold higher than that of wild-type myosin (*12*). The work here shows that these conclusions are correct but that the alterations are far more wide-reaching.

We show that the rate of all nucleotides binding to G680A is reduced 16−30-fold, yet ADP binds 10-fold more tightly to the protein because of a 200-fold reduction in the ADP dissociation rate constant. In contrast both ATP and ADP binding to acto·G680A were fast and indeed are faster than binding to M761-2R. While the ATP affinity to acto·G680A ($\mathbf{K}_1$) is 6-fold tighter, the ADP affinity ($\mathbf{K_{AD}}$) is 180-fold tighter than for M761-2R. Actin did not reduce the affinity of G680A for ADP, as the ratio of $\mathbf{K_{AD}}/K_D$ is close to 1 compared to a value of 14 for M761-2R. As actin binding did not reduce the affinity for ADP, we checked whether actin accelerates the rate of ADP release. ADP release from G680A was estimated from the rate at which mantATP can displace ADP. This gave values of 0.05 s^{-1} for k_{-D} and 3.1 s^{-1} for $\mathbf{k_{-AD}}$, which means that the rate of ADP release is accelerated 3.1/0.05 = 62-fold by actin. Both the rate of nucleotide binding and the rate of release are therefore accelerated by actin.

For G680A the communication between ADP and actin, binding is thus altered such that the two sites are thermodynamically uncoupled but kinetically actin still accelerates ADP release. This suggests that in terms of transition states the energy barrier for binding ADP is reduced by actin but the free energy of binding itself is not altered. This behavior is consistent with a model that requires a transient opening of the nucleotide pocket for nucleotide binding and release to occur. Actin facilitates the opening of the pocket, but the binding of nucleotide within the pocket itself is unaffected. Confirmation of this interpretation will require detailed measurement of the temperature dependence of the rate and equilibrium constants.

The kinetic behavior of G680A is similar to that observed for the truncated motor domain construct M754 (*20*, *32*). For M754 we showed that the affinity of ADP for both M754 and acto·M754 was 0.4 μM, while the ADP dissociation rates were 0.06 and 3.1 s^{-1} for M754 and acto·M754, respectively. The loss of six carboxy-terminal residues leads to a significant destabilization of the M754 protein (*33*); however, we have no indication that point mutations at position G680 have similar consequences. If nucleotide binding requires some opening of the nucleotide pocket, then this opening must be inhibited in the absence of actin for both constructs. M754 displayed a 20-fold reduction in the rate of ATP binding to the free myosin motor, and the second-order rate constants for ATP binding to G680A were 30-fold slower than that observed for the wild-type construct M761-2R. Once the nucleotide has bound, the pocket is more stable in the closed form, leading to more tightly bound nucleotide and slow dissociation rates. In the presence of actin, both ATP and ADP bound faster to the pocket, compatible with actin facilitating pocket opening to allow nucleotide binding. Once bound, ATP induced actin dissociation in the normal way while ADP bound to the pocket tightly but had no effect on actin affinity. Thus, truncation of the myosin motor at position 754 or the point mutation at position 680 leads to thermodynamic uncoupling of ADP and actin affinities. ADP binds tightly to the free and the actin-bound forms of both of the constructs, and actin must bind with similar affinity in the presence and absence of ADP due to the thermodynamic relationship defined by Scheme 3.

ACKNOWLEDGMENT

We thank S. Zimmermann for the generation of expression vectors for the mutant constructs; G. Helmig for the preparation of actin; M. L. W. Knetsch for critical reading of the manuscript; D. R. Trentham for valuable comments and suggestions; and R. S. Goody and K. C. Holmes for continual support and encouragement.

REFERENCES

1. Warrick, H. M., and Spudich, J. A. (1987) *Annu. Rev. Cell Biol. 3*, 379−421.
2. Manstein, D. J. (1993) in *Cell Behaviour: Adhesion and Motility* (Jones, G., Wigley, C., and Warn, R., Eds.) pp 375−381, Company of Biologists Ltd., Cambridge, U.K.
3. Anson, M., Geeves, M. A., Kurzawa, S. E., and Manstein, D. J. (1996) *EMBO J. 15*, 6069−6074.
4. Rayment, I., Holden, H. M., Whittaker, M., Yohn, C. B., Lorenz, M., Holmes, K. C., and Milligan, R. A. (1993) *Science 261*, 58−65.
5. Wells, J. A., Knoeber, C., Sheldon, M. C., Werber, M. M., and Yount, R. G. (1980) *J. Biol. Chem. 255*, 11135−11140.
6. Huston, E. E., Grammer, J. C., and Yount, R. G. (1988) *Biochemistry 27*, 8945−8952.
7. Liang, W., and Spudich, J. A. (1998) *Proc. Natl. Acad. Sci. U.S.A. 95*, 12844−12847.
8. Wells, J. A., and Yount, R. G. (1979) *Proc. Natl. Acad. Sci. U.S.A. 76*, 4966−4970.

9. Dalbey, R. E., Weiel, J., and Yount, R. G. (1983) *Biochemistry 22*, 4696−4706.
10. Titus, M. A., Ashiba, G., and Szent-Gyorgyi, A. G. (1989) *J. Muscle Res. Cell Motil. 10*, 25−33.
11. Kinose, F., Wang, S. X., Kidambi, U. S., Moncman, C. L., and Winkelmann, D. A. (1996) *J. Cell Biol. 134*, 895−909.
12. Patterson, B., Ruppel, K. M., Wu, Y., and Spudich, J. A. (1997) *J. Biol. Chem. 272*, 27612−27617.
13. Sambrook, J., Fritsch, E. F., and Maniatis, T. (1989) *Molecular cloning: a laboratory manual*, Cold Spring Harbor Laboratory Press, Cold Spring Harbor, NY.
14. Manstein, D. J., Schuster, H.-P., Morandini, P., and Hunt, D. M. (1995) *Gene 162*, 129−134.
15. Egelhoff, T. T., Titus, M. A., Manstein, D. J., Ruppel, K. M., and Spudich, J. A. (1991) *Methods Enzymol. 196*, 319−334.
16. Manstein, D. J., and Hunt, D. M. (1995) *J. Muscle Res. Cell Motil. 16*, 325−332.
17. Lehrer, S. S., and Kerwar, G. (1972) *Biochemistry 11*, 1211−1217.
18. Criddle, A. H., Geeves, M. A., and Jeffries, T. (1985) *Biochem. J. 232*, 343−349.
19. Bradford, M. M. (1976) *Anal. Biochem. 72*, 248−254.
20. Kurzawa, S. E., Manstein, D. J., and Geeves, M. A. (1997) *Biochemistry 36*, 317−323.
21. Bagshaw, C. R., Eccleston, J. F., Eckstein, F., Goody, R. S., Gutfreund, H., and Trentham, D. R. (1974) *Biochem. J. 141*, 351−364.
22. Millar, N. C., and Geeves, M. A. (1983) *FEBS Lett. 160*, 141−148.
23. Siemankowski, R. F., and White, H. D. (1984) *J. Biol. Chem. 259*, 5045−5053.
24. Kurzawa-Goertz, S. E., Perreault-Micale, C. L., Trybus, K. M., Szent-Györgyi, A. G., and Geeves, M. A. (1998) *Biochemistry 37*, 7517−7525.
25. Manstein, D. J., Ruppel, K. M., and Spudich, J. (1989) *Science 246*, 656−658.
26. White, H. D. (1982) *Methods Enzymol. 85*, 698−708.
27. Kurzawa, S. E., and Geeves, M. A. (1996) *J. Muscle Res. Cell Motil. 17*, 669−676.
28. Fisher, A. J., Smith, C. A., Thoden, J., Smith, R., Sutoh, K., Holden, H. M., and Rayment, I. (1995) *Biochemistry 34*, 8960−8972.
29. Smith, C. A., and Rayment, I. (1996) *Biochemistry 35*, 5404−5417.
30. Patterson, B., and Spudich, J. A. (1995) *Genetics 140*, 505−515.
31. Patterson, B., and Spudich, J. A. (1996) *Genetics 143*, 801−810.
32. Woodward, S. K., Geeves, M. A., and Manstein, D. J. (1995) *Biochemistry 34*, 16056−16064.
33. Levitsky, D. I., Ponomarev, M. A., Geeves, M. A., Shnyrov, V. L., and Manstein, D. J. (1998) *Eur. J. Biochem. 251*, 275−280.

BI982251E